Individual Tree Parameters Estimation for Plantation Forests Based on UAV Oblique Photography

XUEMEI ZHOU AND XIAOLI ZHANG [ID]

Precision Forestry Key Laboratory of Beijing, Beijing Forestry University, Beijing 100083, China
The Key Laboratory for Silviculture and Conservation of Ministry of Education, Beijing Forestry University, Beijing 100083, China

Corresponding author: Xiaoli Zhang (zhangxl@bjfu.edu.cn)

ABSTRACT The parameters of individual trees in forests are important for accurate forestry inventory and sustainable management. Unmanned aerial vehicle (UAV) oblique photogrammetry technology plays an important role in forest surveys because of its flexibility, low cost, high spatial data resolution. Few studies have committed to extract individual tree parameters and estimate individual tree biomass using oblique photography data. In this study, images of larch(*Larix gmelinii*) and Chinese pine(*Pinus tabuliformis*) plantations with different ages were acquired by UAV oblique photogrammetry. Then, three dimension (3D) point clouds were constructed recovered by the structure from motion (SFM) algorithm and than normalized. The watershed segmentation, point cloud segmentation (PCS) and object-oriented multiresolution segmentation (MRS) methods were used to delineate individual trees and extract tree height and crown area. Finally, stepwise regression was used to fitting individual tree biomass models based on the point cloud metrics, crown area obtained from individual tree segmentation and measured biomass. The results indicated that: most suitable segmentation method are determined for different tree species at different ages; optimal prediction models of individual tree biomass can be constructed by combining the point cloud metrics with the tree crown area obtained by segmentation, accuracy of the models are all greater than 0.8. The results show that UAV oblique photography technology can be used to accurately extract the individual tree parameters of larch and Chinese pine plantation forests in northern China and can meet the requirements of large-scale and low-cost forestry inventory.

INDEX TERMS UAV oblique photography, point clouds, individual tree segmentation, individual tree parameters, individual tree biomass models.

I. INTRODUCTION

Plantation forests account for approximately 7.3% of global forest resources and play an important role in mitigating global climate change, conserving water resources and protecting biodiversity. Accurate and efficient measurement of individual tree parameters is the basis of inventorying plantation forest resources [1]–[3]. Traditional forestry methods require in-depth outdoor ground-level measurements, which are time-consuming, labor-intensive, and inefficient. It is difficult to obtain continuous individual tree parameters over large areas [4], [5]. The proposal of precision

The associate editor coordinating the review of this manuscript and approving it for publication was Geng-Ming Jiang [ID].

forestry poses new challenges to the traditional forestry management model. Efficient acquisition of nondestructive, high-resolution forestry data represents the key to accurate extraction of individual tree parameters [6], [7].

With the rapid development of modern remote sensing technology, it has become possible to obtain large-scale forest information and monitor the growth of trees and the distribution of forest resources quickly and efficiently. Many studies on the extraction of forest parameters have been based on satellite images, but due to the high cost, spatial and spectral resolution, and influence of atmospheric conditions and other factors, the precise acquisition of individual tree parameters remains limited. Segmentation algorithms are the base of individual tree parameters estimation. There are mainly

two kinds of individual tree segmentation methods based on point cloud data: one is based on normalized point clouds, which is called NPC(normalized point cloud) method; the other is based on canopy height model(CHM) generated by point clouds interpolation. NPC method complete the segmentation by setting distance threshold according to spatial location relationship among point clouds, while the method based on CHM detects the tree tops and tree crown by height change of forests canopy surface. There are many image-based segmentation methods, such as edge detection algorithm, region segmentation, image threshold segmentation and so on.

Among the existing remote sensing technologies for forest resource inventories, light detection and ranging (LiDAR) and photogrammetry are two commonly used methods for obtaining 3D forest information [8]–[11]. LiDAR is a detection method that actively emits laser beams. With its advantages of strong penetrability and resistance to weather, it can obtain 3D information on forest canopy structure and terrain with high accuracy. A large number of studies have shown that the point clouds generated by LiDAR can accurately obtain forest scale and individual tree scale structure information, such as tree height, crown area and biomass [12], [13]. However, LiDAR does not include spectral and textural information, and the acquisition cost is relatively high, making it difficult to use for continuous monitoring of forest growth. Unmanned aerial vehicle (UAV) oblique photogrammetry technology is a high-precision remote sensing measurement technology that has been rapidly developed in recent years. It has gradually been applied to forest parameter extraction and continuous monitoring of forest growth and features advantages such as low cost and high flexibility [14]–[16]. Compared with LiDAR, oblique photography can not only obtain high-resolution, high-overlap images but also reconstruct high-density point clouds, so it can more accurately characterize forest canopy information, realize the visualization of complex forest structures and reduce the possibility of missing treetops due to insufficient point clouds density. In addition, the acquired images have rich textural information, which can effectively preserve the canopy edge information and has a unique advantage in extracting the crown area accurately [17]–[20].

Jensen et al. (2016) extracted the height of sparse mixed forest in Texas in the United States by using three-dimensional point clouds produced from UAV high-resolution images ($R^2 > 0.89$), which yielded results similar to those based on UAV-LiDAR [21]. Goodbody et al. (2017) used LiDAR and point clouds to estimate the stem volume of a spruce forest in western Canada. In that study, a digital elevation model (DEM) extracted from the LiDAR data was used to normalize the point clouds, and the prediction model was then constructed by the metrics extracted from UAV-acquired stereo-photogrammetric point clouds and the measured values of the sample plot (rRMSE = 18.5%) [22]. Giannetti et al. (2018) tested the accuracy of estimating forest volume by using unnormalized

digital aerial photography (DAP) point cloud metrics in a coniferous forest on a plain in Norway and in temperate mixed forests in a mountainous area in Italy [23]. The results showed that the forest volume can also be estimated accurately by using unnormalized DAP point cloud metrics (rRMSE = 15.9%-17.9%). Hernández et al. (2017) used multitemporal high-resolution image data to monitor the dynamic growth of golden pine plantations in central Portugal and extracted the height and crown area of individual tree at different times. The final estimation result of tree height had an R^2 of 0.96 [24]. Lin et al. (2018) used UAV oblique photography to extract individual tree height and estimate aboveground biomass of subalpine sparse coniferous forests in Sichuan, China, and the research results showed that oblique photogrammetry has good accuracy in estimating tree height and biomass (RMSE = 1.77 m and 54.9 kg, respectively) [25].

The above studies show that UAV oblique photogrammetry technology can be efficiently and accurately applied to forest resource monitoring and sustainable management. Oblique data can not only generate point clouds similar to LiDAR to describe the 3D information of forests, but also have spectral information. However, most of the studies were based on point clouds and did not consider the role of spectral information. Point clouds metrics were used when estimating biomass, and other parameters (such as crown area, crown shape, etc.) were not considered. Besides, most of the studies were conducted at the stand scale and involved mostly sparse forestland [26], [27]; few of them set individual trees as the research object, and there was no systematic comparison of the application effects of different segmentation algorithms for different densities, terrains, age classes, tree species and other situations, resulting in a lack of scalability and practicality. The research goal of this paper is to use the 3D information in point clouds and the spectral information of the images to determine the algorithms suitable for extracting individual tree parameters, and estimate individual tree biomass using parameters and point cloud variables. In this study, the typical plantations in northern China were taken as the research object, and the application potential of UAV oblique photography technology in the investigation of plantation resources is explored. By constructing the technical framework of automatic extraction of individual tree structure parameters, the adaptability of tree species segmentation algorithm for different forest ages is explored, which provides a new way for low-cost and high-precision forest investigation.

II. MATERIALS AND METHODS

In order to extract the parameters of individual tree, structure from motion (SFM) algorithm was used to restore the point clouds of original UAV oblique images. Tree height and crown area of individual trees were estimated by segmenting normalized point cloud, CHM and orthophoto. Multiple stepwise linear regression was used to construct individual tree biomass models in different forest stands based on the
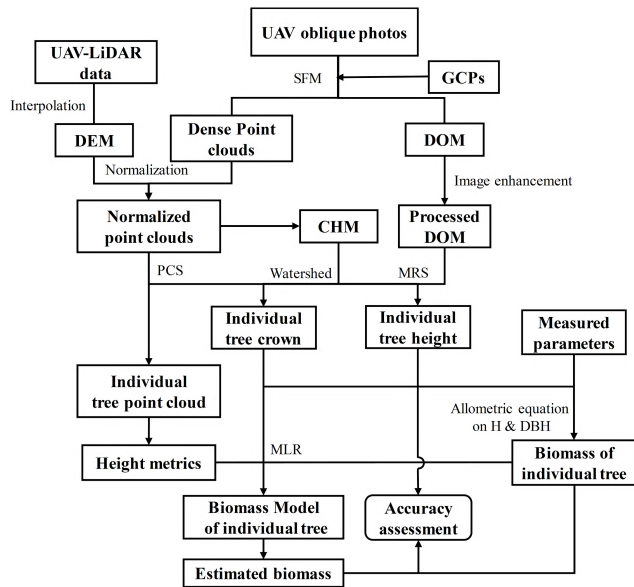
FIGURE 1. Flowchart of individual tree parameters estimation. SFM: structure from motion; GCPs: ground control points; DEM: digital elevation model; DOM: digital orthophoto map; PCS: point cloud segmentation; MRS: multi-resolution segmentation; MLR: multiple linear regression; H: tree height; DBH: diameter at breast height.

point cloud metrics, crown area obtained from individual tree segmentation and measured biomass. Flowchart of individual tree parameters estimation is shown in Figure 1.

A. STUDY AREA AND FIELD MEASUREMENTS

The study area is located in the Wangyedian experimental forest farm (118°09' ∼ 118°30' E, 41°35' ∼ 41°50' N) in Karaqin Banner, Chifeng city, Inner Mongolia, China. The elevation range of this mountainous is 200 ∼ 400 m, and the slope is 15∼35° with complicated terrain conditions. The annual average temperature is 7.4 °C, and the annual average rainfall is 300-500 mm. The forest coverage in the study area reaches 80%, and the vegetation types are diverse. There are four mainly dominant tree species, including larch (*Larix gmelinii*), Chinese pine (*Pinus tabuliformis*), spruce (*Picea asperata Mast.*) and birch (*Betula platyphylla Suk.*). Among them, larch and Chinese pine are the main tree species, accounting for more than 90% of the planted area of the plantation forests. The location of the study area and the sample plot distribution are shown in Figure 2.

To ensure that the sample plots are uniformly distributed and representative, systematic sampling was performed in the Wangyedian area of Chifeng city, and the area was divided into 22 grids with a size of 4km × 4km. Considering comprehensive factors such as tree species, forest age, and planting density, six representative grids were selected. Within each area, a square sample plot of 25 m × 25 m was set up. In this study, 2 mature larch plots (L1, L2), 1 young larch plot (L3), 2 mature Chinese pine plots (P1, P2) and 1 young Chinese pine plot (P3) were selected to analyze the suitability of UAV oblique photography for extracting individual tree
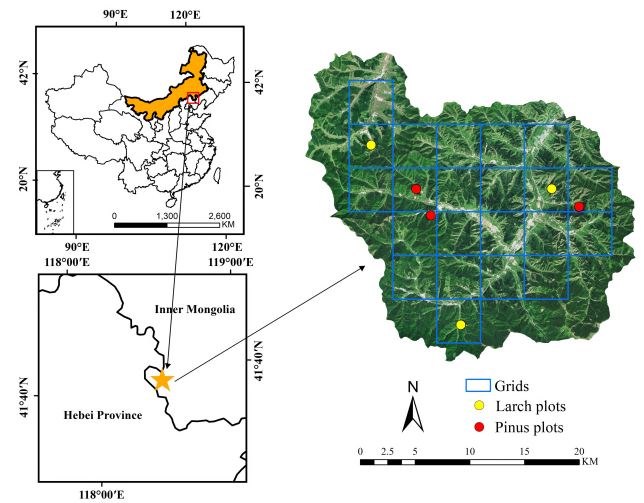
FIGURE 2. Study area and position of sample plots.

parameters for trees of different ages. Field measurements were conducted from September 10-17, 2019. Trees with a diameter at breast height (DBH) greater than 5 cm in the plots were measured to determine position and certain parameters, including tree height, branch height, DBH and crown width. The total tree height were measured with a Vertex V® ultrasonic laser altimeter, DBH was measured by the breast diameter ruler at 1.3 m of the tree trunk on the uphill slope, crown width was determined by the longest distance between the north-south and east-west directions of the canopy by a tape measure. The position of an individual tree was determined with Sanding STS-722 tripod laser total station. The total station was located at a known point and used another known point for orientation. The laser was emitted to height of 1.3m of individual tree to obtain its position, the vertical accuracies were within ± 10 cm. Other information, such as slope, slope direction and canopy cover, were recorded at the same time. The parameters of individual trees and the stand density in the sample plots are shown in Table 1.

B. LiDAR DATA ACQUISITION AND PREPROCESSING

LiDAR data were acquired during September 15-18, 2019. An Rc6-2000 UAV was equipped with a RIEGL vux-1 LiDAR sensor to acquire data within the sample area. The overall point density is better than 25 points/m^2. We removed the noise points of the original data with the height threshold, then aligned LiDAR points through boresight calibration. The point clouds after noise removal and air belt splicing were classified to distinguish ground points, vegetation, buildings and other features. Then, the ground points were interpolated with inverse distance weight (IDW) to generate a DEM with a resolution of 0.2 m.

C. UAV OBLIQUE PHOTOGRAPHY DATA ACQUISITION AND PREPROCESSING

UAV oblique photography data were obtained under sunny and windless conditions during September 23-27, 2019.

**TABLE 1.** Summary of measured sample plot parameters.

Sample plot	Tree species	DBH（cm）	Tree Height (m)	Stem Density (n·ha⁻¹)
L1	Mature Larch	14.8±7.3	14.1±4.9	1504
L2		17.7±6.6	20±4.1	1504
L3	Young Larch	12.0±6.9	11.1±4.4	2224
P1	Mature Chinese pine	24.6±14.7	14.7±7.6	528
P2		25.3±14.2	16.8±6.8	496
P3	Young Chinese pine	15.1±8.3	10.6±5.6	1872

DBH: diameter at breast height

A DJI M600 Pro six-rotor UAV equipped with a five-lens JHP QX3MINI camera (1 vertical and 4 oblique lenses) collected high spatial resolution RGB images of the study area. The UAV had its own positioning system, and the flight height range was 150-250 m, which was same as LiDAR data acquisition and determined according to the altitude difference between the UAV and the hillside on which the sample plots were located. The course overlap was not less than 80%, and the side overlap was not less than 70%. A total of six flights were carried out, each flight time was 15-20 minutes and obtained 2000-2500 images. In addition, in each plot area, 6 ground control points (GCPs) were uniformly arranged around each plot to ensure that they were clearly visible in the images [28]. The flights were completed within three hours before and after noon to reduce the shadow effect of the solar altitude angle. The geographical coordinates and elevation of the GCPs were measured by real-time kinematic (RTK) GPS measurements. The horizontal and vertical accuracies were within ± 3 cm. The layout and measurement of ground control points are shown in Figure 3.

The structure from motion (SFM) technique is an algorithm that can reconstruct 3D structure from a large number of unordered photos. First, the focal length information was extracted from the images, then feature detection and matching were carried out, and the camera orientation and scene geometry information were automatically solved by iterative bundle adjustment [29]. After adding ground control points for geometric precision correction, a nonlinear least square algorithm was used to continuously optimize and generate sparse point clouds. Finally, dense point clouds with absolute coordinates were generated by pixel matching through a dense matching algorithm.

The point clouds generated by 3D reconstruction were interpolated by the IDW algorithm to generate a digital surface model (DSM) with a resolution of 0.2 m. The stitching
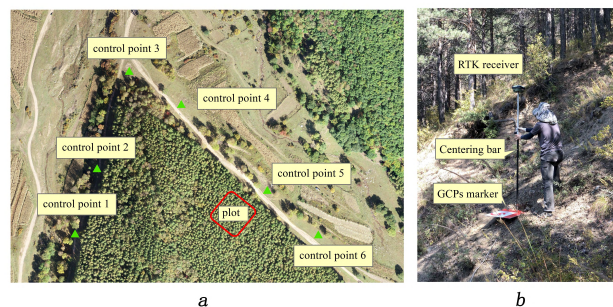
FIGURE 3. Layout and measurement of ground control points (GCPs): (a) The relative position of the GCPs and the sample plot,(b) measuring the absolute coordinates of the GCPs with RTK GPS measurements.

line was selected for the orthophoto with absolute coordinates and high overlap, and mosaicking was carried out to obtain an orthophoto in each survey area with a resolution of 5 cm. The 3D reconstruction and orthophoto generation in this study were completed in Context Capture software.

D. REGISTRATION

The 3D point clouds recovered from oblique photography images had absolute geographical coordinates, but they still deviated from LiDAR data. In each flight area, several identical ground objects with obvious characteristics, such as roofs and road intersections, were selected from the point clouds of oblique photography and LiDAR data for manual registration. After point cloud registration, the error range was controlled to within 0.2 m, which can meet the requirements of individual parameter extraction.

The DEM generated from the LiDAR data was used to normalize the point clouds after registration and DSM generation [30], and the normalized point clouds and CHM were obtained. The normalized point clouds, CHM and orthophoto were clipped using the boundary of the sample plots.

E. SEGMENTATION ALGORITHMS AND ACCURACY INDICATORS

1) WATERSHED

The watershed algorithm is a kind of mathematical morphology segmentation method based on topological theory [31], [32]. The gray value of each pixel in the image represents the altitude of that point, and each local minimum and its area of influence become a watershed. First, the gray level of each pixel is sorted from low to high, and then the catchment basin is constructed according to the gray value during the merging process to obtain the canopy boundary. Because of the sudden change caused by holes or noise in the CHM, the watershed method often exhibits oversegmentation. Therefore, smoothing processing involving a Gaussian filter and setting of a minimum tree height threshold is carried out for the CHM. The larger the Gaussian smoothing factor is, the higher the smoothness degree is, and the smoothness degree affects the number of individual segmented trees. If there is oversegmentation, the smoothing factor should be

increased. The smoothing window size is generally set as large as the average crown width. Trial and error revealed that using Gaussian smoothing factors of 0.7 and 0.5 and window sizes of 5 × 5 and 3 × 3 were optimal for mature and young larch forests, respectively, and that using Gaussian smoothing factors of 1.3 and 1.0 and window sizes of 7 × 7 and 5 × 5 were optimal for mature and young Pinus forests, respectively. The watershed segmentation algorithm of this study was implemented in software MATLAB R2017a. The maximum pixel value was taken as the height of an individual tree in the range of the canopy boundary.

2) POINT CLOUD SEGMENTATION (PCS)

The principle of the point cloud segmentation (PCS) algorithm involves regional growth combined with a distance threshold[33]. The PCS algorithm divides the normalized point clouds into individual trees and uses the location information contained in all point clouds directly. The algorithm makes full use of the fact that there is a certain distance between trees, especially between treetops. First, the highest point in the normalized point clouds is taken as the starting point and is considered the treetop of the first tree. Then, the first tree is identified on the basis of the first treetop by judging the distance between the surrounding points and the growth area. Finally, all individual trees are segmented by iteration. Compared with the watershed algorithm, the advantage of PCS is that it can directly use the height and position information of point clouds to avoid the reduction of segmentation accuracy caused by the error in the process of interpolation. In this study, according to the characteristics of tree species and forest age, the distance thresholds for mature larch and Chinese pine were set to 2 m and 3 m, respectively, and those of young larch and Chinese pine were set to 1 m. PCS was implemented with package lidR in software RStudio.

3) MULTIRESOLUTION SEGMENTATION (MRS)

The object-oriented multiresolution segmentation (MRS) algorithm is based on fuzzy mathematics. The statistics of the grayscale, size, and texture of multiple pixels of the object in the image are calculated to obtain the probability that the object belongs to a certain category [34]. On the premise of maintaining the maximum feature similarity between similar pixels, the image is segmented at different scales. The correct setting of scale and shape parameters is the basis of the ideal effect of MRS. The threshold of heterogeneity between objects is determined by scale parameters; the larger the scale parameters, the larger the average area of the segmentation unit. The determination of the shape parameters depends on the regularity of the shape of the features. To enhance the contrast between the ground and the tree crown, a linear grayscale transformation in the spatial domain of the original image was performed in this study [35]. After the first MRS of the enhanced image, the object units in the image were merged to ensure the minimum heterogeneity between the objects. Based on the results of the first multiscale segmentation,

TABLE 2. Algorithm rules and parameter settings.

MRS	Parameters	Mature Larch	Young Larch	Mature Chinese Pine	Young Chinese Pine
1st	scale	20	15	20	15
	shape	0.9	0.9	0.9	0.9
	compactness	0.8	0.7	0.8	0.9
2nd	scale	55	35	100	40
	shape	0.9	0.9	0.8	0.8
	compactness	0.5	0.7	0.9	0.9

the nearest neighbor classification of the rule set was used to distinguish the crown and the ground for each object after segmentation. The samples of the ground background and the crown were selected by visual interpretation, and the band mean value was configured as the nearest neighbor feature for classification [36]–[38]. Based on merged tree crown object, MRS was carried out again to obtain the ideal individual segmentation result. The segmentation parameters set for different forest ages, tree species and average crown sizes are shown in Table 2. MRS was implemented in software eCognition Developer 64 8.7.

Taking the measured position of an individual tree as the center and the average value of the measured crown width in the north-south and east-west directions as the diameter for circular buffering, the accuracy of the results is judged based on the crown boundary obtained by segmentation. The number of correct crowns (N_T), the number of missing crowns (N_O) and the number of oversegmented crowns (N_C) were selected for evaluation. If the overlapping area of the circular buffer zone and the segmented crown accounts for more than 50% of each or one of the two, then the crown is judged to be correctly segmented. If there is more than one circular buffer in the segmented crown or there is no segmented crown for more than 50% of the area of the buffer zone, then the crown is judged to be missing. If multiple segmented tree crowns appear in the circular buffer, the crown is judged to be oversegmented [39].

Three indicators were used to evaluate the accuracy of individual tree segmentation, and the formulas were as follows:

$$r = \frac{N_T}{N_T + N_O} \qquad (1)$$

$$p = \frac{N_T}{N_T + N_C} \qquad (2)$$

$$F = \frac{2(r \times p)}{r + p} \qquad (3)$$

r represents the individual tree detection rate, *p* represents the detection accuracy rate, and *F* represents the overall accuracy. N_T is the number of individual trees obtained by segmentation and matched with the measured data, N_O is the number of individual trees that cannot be segmented but do exist in the measured data, and N_C is the number of

TABLE 3. Biomass growth equation of different tree species.

Tree Species	Model	R^2
Mature Larch	$\ln(Y) = -2.2372 + 0.8082 \ln(D^2 H)$	0.98
Young Larch	$Y = 0.0712 \times (D^2 H)^{0.8902}$	0.98
Mature Chinese Pine	$Y = 0.1106 \times (D^2 H)^{0.8512}$	0.99
Young Chinese Pine	$Y = 0.14 \times (D^2 H)^{0.8203}$	0.97

individual trees that have been segmented but do not exist in the measured data [40], [41].

F. INDIVIDUAL TREE BIOMASS MODELS

In this study, the measured DBH and tree height were substituted into an allometric equation to obtain the biomass of individual trees, which was taken as the measured value. Stepwise regression was used to fit the biomass models of mature and young larch and Chinese pine with 13 height metrics, segmented tree crown and measured biomass [42].

Referring to the Comprehensive Database of Biomass Regressions for China's Tree Species (2015) [43], allometric equations suitable for mature and young larch and Chinese pine were determined according to the conditions of tree species, age and density, and then the measured DBH and tree height of individual trees were substituted to calculate the measured biomass. The allometric growth equations based on DBH and tree height are shown in Table 3.

Multiple height metrics were calculated from individual tree point clouds. In this study, 14 metrics were selected, among which 13 were height metrics and 1 was the segmented crown area. The metrics and descriptions are shown in Table 4.

Seventy percent of the measured biomass of individual trees in sample plots was selected randomly as the dataset for biomass model fitting. The linear equation constructed by the stepwise regression method is used to estimate the biomass of individual trees. The model form is as follows:

$$y = b_0 + b_1 q_1 + b_2 q_2 + \ldots + b_n q_n + \varepsilon \quad (4)$$

In the model, y is the biomass of an individual tree, q is the independent variable, b is the constant, and ε is the error.

G. ACCURACY EVALUATION INDICATORS

In this study, the coefficient of determination (R^2), root mean square error (RMSE) and relative root mean square error (rRMSE) are used to evaluate the accuracy of height detection and the biomass model of individual trees. Additionally, RMSE and rRMSE are used to evaluate the accuracy of the crown area. The circular area obtained from the diameter of the average crown width in the north-south and

east-west directions was taken as the measured crown area. The formulas are as follows:

$$R^2 = 1 - \frac{\sum_{i=1}^{n} (\hat{x}_i - \bar{x})^2}{\sum_{i=1}^{n} (x_i - \bar{x})^2} \quad (5)$$

$$RMSE = \sqrt{\frac{1}{n} \sum_{i=1}^{n} (x_i - \hat{x}_i)^2} \quad (6)$$

$$rRMSE = \frac{RMSE}{\bar{x}} \times 100\% \quad (7)$$

In the formulas, x_i is the measured value, $\hat{x}_i$ is the estimated value, and $\bar{x}$ is the measured average value.

III. RESULTS

A. POINT CLOUD REGISTRATION, IMAGE ENHANCEMENT AND CLASSIFICATION

Taking the point clouds recovered from 3D reconstruction of oblique images as the reference point clouds, the LIDAR point clouds are used as the registration point clouds. Obvious feature points. such as roofs and intersections, are selected manually in the overlapping area. After registration, the horizontal error was less than 0.2 m, and the vertical error was less than 0.1 m, which meets the requirements of individual tree parameter extraction. The normalized point clouds after registration are shown in Figure 4.

The original images generated by oblique photography have gray concentrations, and the local brightness value is too high. Gray linear stretching of the spatial domain was applied to the orthophoto images, which increased the difference between the crown and the ground to facilitate the subsequent classification and individual tree crown segmentation. The images were classified into two categories-the crown and the ground-by the nearest neighbor classification method to eliminate the possible influence of the background value on the segmentation. The results of image enhancement and classification are shown in Figure 5.

B. SEGMENTATION RESULTS AND ACCURACY EVALUATION

In watershed segmentation, the CHM generated by point cloud interpolation was used as the base image, the segmentation boundary was used as the crown edge, and the maximum pixel value of the CHM within the boundary was

FIGURE 4. Display of point cloud registration results. The colored points represent the oblique photography point cloud, and the red points represent the LiDAR point cloud.

TABLE 4. Description of metrics derived from UAV oblique photography point clouds data.

| Metrics	Description
Crown area	The crown area of individual tree segmented
H_{aad}	The average absolute deviation of all points $$V = \frac{\sum_{i=1}^{n}(|z_i - \bar{z}|)}{n}$$ z_i represents the elevation of ith point with a statistical unit, $\bar{z}$ represents the average elevation of all points within a statistical unit, and n is the number of points in a statistical unit.
H_{a75}, H_{a95}	The cumulative height of $X\%$ points in each statistical unit is the statistical unit's $H_{aX.}$
H_{cv}	The coefficient of variation of height of all points after normalized (the ratio of thestandard deviation to the mean)
H_{IQ}	The height percentile interquartile distance, difference elevation between 75th and 25th
$H_{kurtosis}$	The kurtosis of the heights of all points by first echo
$H_{max}, H_{mean}, H_{median}$	The maximum,mean,median height of all points after normalized
H_{75}, H_{95}	The percentiles of the canopy height distributions(75th,95th)
H_{smean}	The generalized means for the 2nd power $$V = \sqrt{\frac{\sum_{i-1}^{n} z_i{}^2}{n}}$$ Z is the H value of the i point in a statistical unit.
H_{std}	The standard deviation of height for all points after mormalized
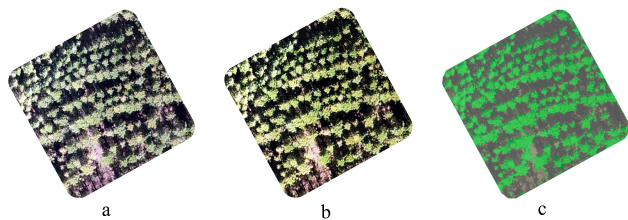
FIGURE 5. Image enhancement and classification: (a) the orthophoto image of the sample plot generated by oblique photogrammetry, (b) an enhanced view of the image, (c) the result of tree crown and ground classification (green is the tree crown, translucent gray is the ground background).

considered the treetop. The results of PCS were presented in a 3D view of the normalized point cloud, and the trees were rendered according to different colors. The results of MRS used the orthophoto image after enhancement as the base image and the segmented object boundary as the crown edge. The segmentation results for larch and Chinese pine are shown in Figure 6 and Figure 7, and the segmentation accuracy statistics are shown in Table 5.

Evaluation indicators show that the PCS method performs best in the individual tree segmentation of larch (average F-score = 0.94), and MRS and PCS yield similar segmentation results for young larch. The crown shape of larch is relatively regular, the gap between adjacent trees is relatively clear, and the height of individual trees is relatively close to the average. The SFM method has a high accuracy of feature

point matching, so setting a suitable point cloud distance threshold can achieve a good segmentation effect.

The evaluation indicators show that the watershed method performs best in the individual tree segmentation of Chinese pine (average F-score = 0.89), and the accuracy of MRS is lower than that of the other two methods. Part of the crown branches of Chinese pine are flat, and the crowns of adjacent trees overlap. This caused the number of mismatched points to increase in the process of point cloud restoration. The watershed algorithm performs better than the PCS method in segmentation when the CHM is smoothed by a Gaussian filter.

The PCS method is suitable for individual larch segmentation and has the highest accuracy (average F-score = 0.94); furthermore, the segmentation accuracy of mature larch is higher than that of young larch. The watershed algorithm is suitable for individual Chinese pine segmentation and has the highest accuracy (average F-score = 0.89); additionally, the segmentation accuracy of mature Chinese pine is higher than that of young larch. The same method has different segmentation accuracies for larch and Chinese pine. Under the three different segmentation methods, the segmentation results of larch are all greater than those of Chinese pine. The tree heights of Chinese pine vary, and the branches are flat. Because the upper part of the tree canopy could not be detected, undersegmentation occurred, and the overall segmentation accuracy for Chinese pine was lower than that for larch.
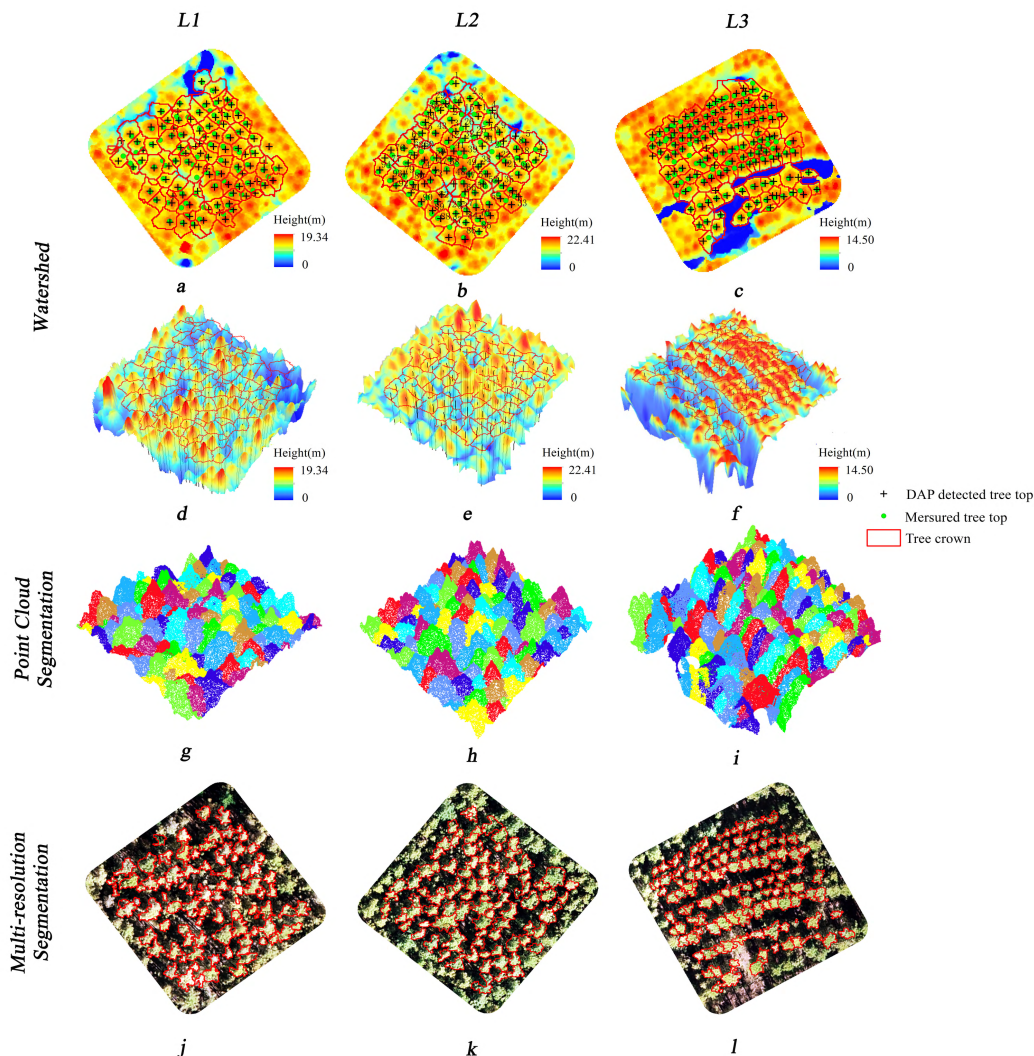
FIGURE 6. Results of individual larch segmentation. (a),(b), (c), (d), (e), and (f) are the results of individual tree segmentation based on the watershed algorithm; the edge of the tree crown is represented by a red boundary, and the detected treetop and measured treetop are marked. (a), (b) and (c) are in planar view; (d), (e) and (f) are in 3D view. (g), (h) and (i) are the segmentation results based on PCS; (j), (k) and (l) are the segmentation results based on MRS.

C. EXTRACTION RESULTS AND ACCURACY EVALUATION OF THE HEIGHT AND CROWN AREA OF INDIVIDUAL TREES

The maximum value of CHM pixels in the individual tree crown boundary was obtained by the watershed method, and the maximum elevation of normalized point clouds was extracted as the tree height in the individual tree crown boundary by the PCS method. The average RMSE for larch and Chinese pine was 0.79 m, and the rRMSE was no higher than 5.0%; the average RMSE of young larch and Chinese pine was 1.25 m, and the rRMSE was no higher than 12.2%.

The estimated tree height is linearly correlated with the measured tree height. With the watershed and PCS methods, the extracted tree height accuracy of mature larch and Chinese pine is greater than that of young larch and Chinese pine. For mature stands, the height accuracy of larch and Chinese pine extracted by PCS method is higher than that by the watershed algorithm; for young stands, the height accuracy of the watershed and PCS methods differs between the two species: for the tree height extraction of young larch, the accuracy of the watershed method is higher than that of the PCS method, while for the tree height extraction of young Chinese pine, the accuracy of the watershed algorithm is lower than that of PCS method. The results show that the PCS algorithm is suitable for extracting individual tree heights of mature larch, mature Chinese pine and young Chinese pine and that the watershed algorithm is suitable for extracting individual tree heights of young larch.

For larch and mature Chinese pine, the watershed algorithm has the best performance in extracting the individual tree crown area; for young Chinese pine, the PCS method works best. The crown area acquired by field measurement
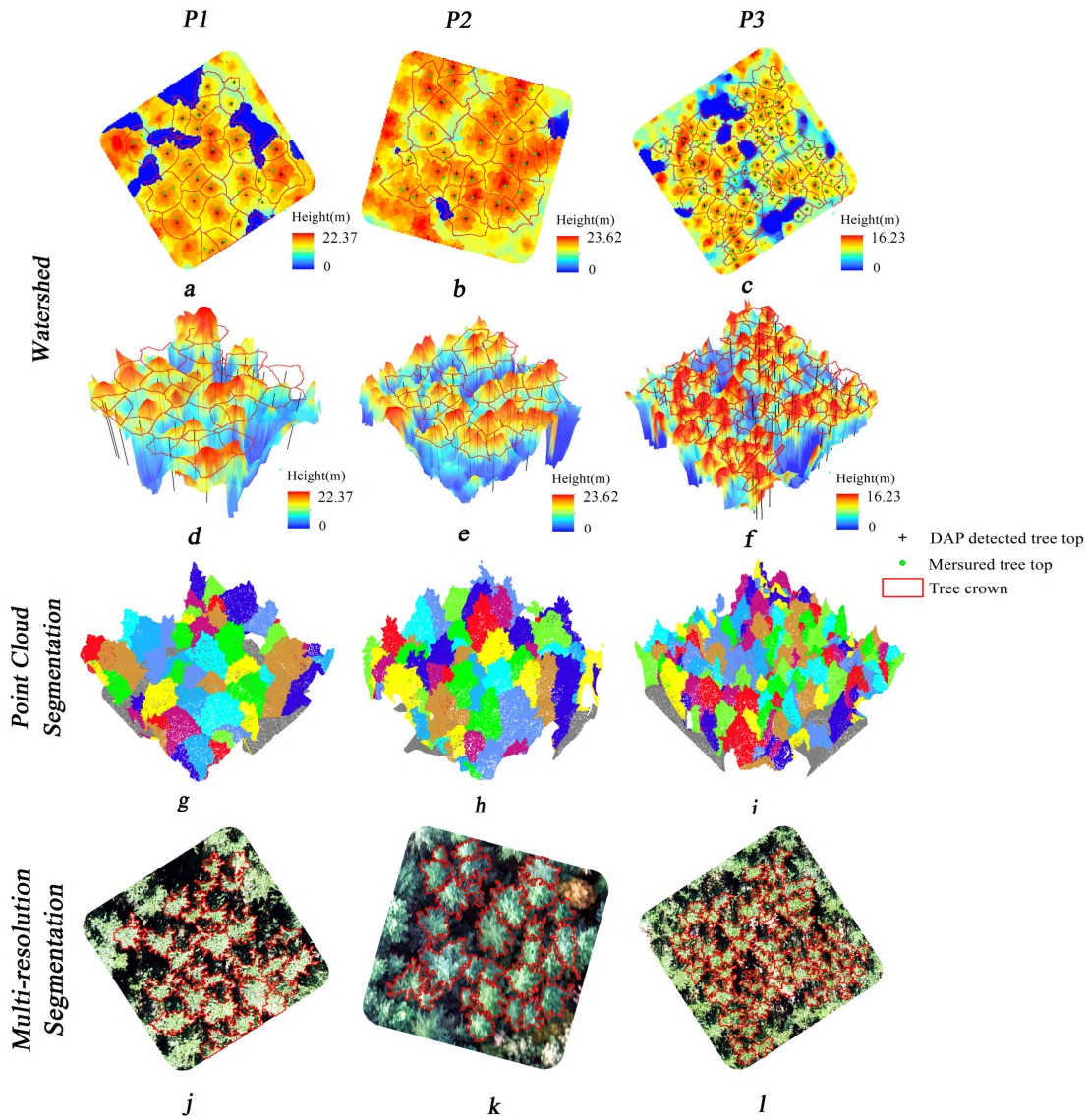
FIGURE 7. Results of individual Chinese pine segmentation. (a),(b), (c), (d), (e), and (f) are the results of individual tree segmentation based on the watershed algorithm; the edge of the tree crown is represented by a red boundary, and the detected treetop and measured treetop are marked. (a), (b) and (c) are in planar view; (d), (e) and (f) are in 3D view. (g), (h) and (i) are the segmentation results based on PCS; (j),(k) and (l) are the segmentation results based on MRS.

and extracted by the watershed, PCS, and MRS methods are shown in Figure 9, and the accuracy comparison is shown in Table 6. The borders of larch and mature Chinese pine are relatively clear, and the height fluctuation information of the crown can be better preserved in CHM smoothed by the Gaussian filter. The LiDAR point clouds have penetrating capability, and echo information of some low vegetation below the forest canopy might cause inaccurate forest crown edges. The extracted crown area of young larch and Chinese pine by the MRS algorithm is significantly smaller than the values extracted by the other two methods and the measured values. The reason may be related to the small canopy of the young forests and the calculation method of the measured crown area.

D. INDIVIDUAL TREE BIOMASS MODEL AND ACCURACY EVALUATION

Seventy percent of individual trees were randomly selected as training samples from mature larch plots (L1 + L2), young larch plots (L3), mature Chinese pine plots (P1 + P2), and young Chinese pine plots (P3). Stepwise regression was used to select the metrics that fit the biomass of larch and Chinese pine at mature and young ages, respectively. The results are shown in Figure 10, which shows that the crown area metrics have a good contribution to all the biomass models. The adjusted R^2 of the optimal models is between 0.79-0.84, which indicates that the fitting effect of the models is good.

The biomass models and accuracy evaluation for larch and Chinese pine at mature and young ages are shown in Table 7.

TABLE 5. The accuracy assessments for three individual tree segmentation algorithms in sample plots.

Sample Plot	Indicator	Watershed	PCS	MRS
L1	r	0.93	0.96	0.94
	p	0.91	0.97	0.93
	F	0.92	0.96	0.93
L2	r	0.90	0.94	0.86
	p	0.94	0.93	0.87
	F	0.92	0.93	0.87
L3	r	0.85	0.94	0.92
	p	0.97	0.94	0.96
	F	0.90	0.94	0.94
P1	r	0.88	0.79	0.94
	p	0.91	0.87	0.76
	F	0.89	0.83	0.84
P2	r	0.87	0.84	0.90
	p	0.96	1.00	0.72
	F	0.92	0.91	0.80
P3	r	0.84	0.74	0.80
	p	0.87	0.91	0.78
	F	0.85	0.82	0.79

TABLE 6. The accuracy assessments for extracted crown area of individual tree.

Sample Plot	Indicator	Watershed	PCS	MRS
L1	RMSE(m^2)	1.14	2.36	2.29
	rRMSE	15.1%	32.0%	28%
L2	RMSE(m^2)	2.55	3.18	3.80
	rRMSE	31.3%	37.4%	33.2%
L3	RMSE(m^2)	1.28	1.62	2.16
	rRMSE	25.7%	32.1%	43.0%
P1	RMSE(m^2)	5.67	6.61	10.18
	rRMSE	21.2%	24.7%	37.8%
P2	RMSE(m^2)	4.93	5.64	6.27
	rRMSE	20.6%	23.6%	26.2%
P3	RMSE(m^2)	3.21	3.11	5.66
	rRMSE	34.6%	33.5%	51.2%

The R^2 values are all greater than 0.8, and the rRMSE values are 14.03%, 11.76%, 13.26% and 13.85%, respectively.

The remaining 30% of individual trees are treated as the validation sample and substituted into the fitted prediction model of individual tree biomass. The validation results are shown in Figure 11. The results show that the validation R^2 is greater than 0.84, and the rRMSE is between 9.9% and 18.2%. The point cloud height metrics and crown area are used to fit the biomass model of individual trees with high accuracy.

IV. DISCUSSION
A. THE FEASIBILITY AND PRACTICABILITY OF EXTRACTING INDIVIDUAL PARAMETERS BY UAV OBLIQUE PHOTOGRAPHY
One of the purpose of this study is to explore the potential of UAVs equipped with oblique cameras to accurately extract individual tree parameters. Therefore, we obtained hundreds of high-overlap high-resolution photos, successfully restored three-dimensional point clouds in the survey area using the SFM technique and generated orthophoto images. Through

individual tree segmentation, the height and crown area of larch and Chinese pine trees in stands of different ages in northern China were estimated efficiently and accurately. The prediction model correlated point cloud height metrics, crown area and individual tree biomass was established, and segmentation methods suitable for estimating individual tree parameters of larch and Chinese pine in stands of different ages were determined. Studies have proven that increasing the density of point clouds can effectively improve the accuracy of detecting treetops and extracting tree height. This study reached a similar conclusion. Lin *et al.* (2011) and Wallace *et al.* (2012) found that high-density point clouds can significantly reduce the underestimation of tree height and the estimation error of single tree parameters through comparative analysis [44]. Zarco Tejada *et al.* (2014) analyzed olive tree images obtained by a fixed-wing UAV and extracted the tree height from a DSM generated from the reconstructed high-density point clouds [45], and the results had a good correlation with the measured tree height (R^2 = 0.83, RMSE = 35 cm). Therefore, point clouds acquired by UAV oblique photography have great potential in extracting the height of a single tree due to their high-density characteristics [46]. In addition, images acquired by UAV oblique photography can also provide information on the color and texture of forest canopies, whereas LiDAR cannot [47]; this information provides more data with which to segment individual tree crowns [48], [49]. The high-resolution characteristics of orthophoto images make up for the shortcomings of traditional remote sensing images in precision forestry inventories. This study explored the ability of individual tree parameter extraction and the adaptability of segmentation algorithms to stands of different ages and plantation densities of larch and Chinese pine in northern China. Subsequent studies should increase the amount of data and detect the applicability of oblique photography techniques to different areas, tree species, natural forests and secondary forests.

B. COMPARISON OF SEGMENTATION ALGORITHM ACCURACY BETWEEN LARCH AND CHINESE PINE OF DIFFERENT AGES
In this study, we selected the watershed, PCS and MRS methods for individual tree segmentation. The results show that the PCS algorithm is suitable for individual larch segmentation with the highest accuracy (average F-score = 0.94), which may be because the larch crown is oval and cone-shaped and the width is relatively uniform. This result is similar to that of Li *et al.* (2012), who successfully used LiDAR point clouds to segment individual trees of coniferous broad-leaved mixed forest, with a detection accuracy of 90% [33]. The results show that the point clouds acquired by oblique photography can be used to segment the mature larch effectively. The watershed method performs best in the individual tree segmentation of Chinese pine (average F-score = 0.89). Some crown branches of Chinese pine are flat, and the crowns of adjacent trees overlap. This caused the number of mismatched points to be relatively high in

TABLE 7. The fitting biomass model and accuracy evaluation of different tree species.

Tree Species	Model	R^2	RMSE(Kg)	rRMSE
Mature Larch	$-118.16+4.12\times Crownarea$ $-38.84\times H_{median}+49.8\times H_{75}$	0.84	13.72	14.03%
Young Larch	$-112.96+3.028\times Crownarea$ $-10.09\times H_{a75}+23.3 H_{max}$	0.81	8.96	11.76%
Mature Chinese pine	$-708.34+9.58\times Crownarea$ $-62.59\times H_{median}+114.63\times H_{75}$	0.87	59.71	13.26%
Young Chinese pine	$-164.6+6.8\times Crownarea$ $-30.28\times H_{a95}-9.87\times H_{mean}$	0.85	13.6	13.85%
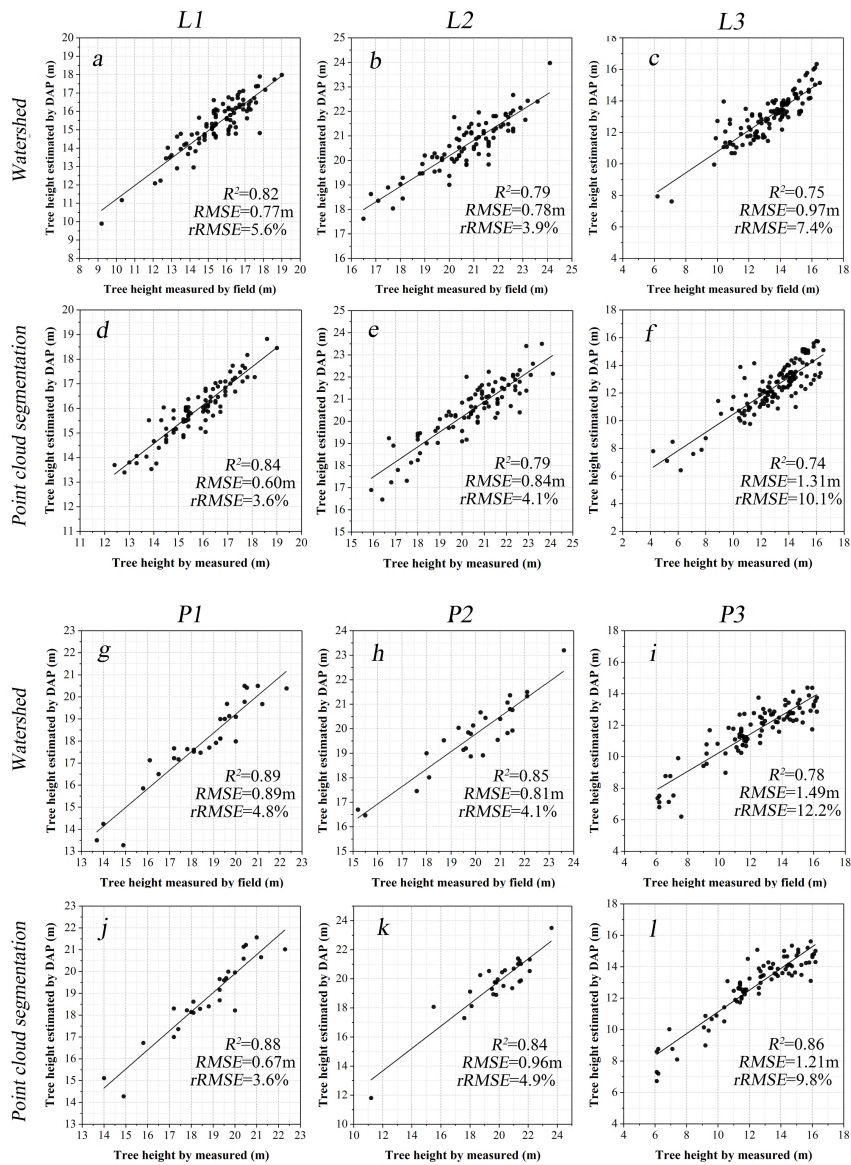
FIGURE 8. Accuracy of individual tree height in different sample plots. (a), (b) and (c) and (d), (e) and (f) are the results of individual larch segmentation based on watershed and PCS, respectively; (g), (h), and (i) and (j),(k) and (l) are the results of individual Chinese pine segmentation based on watershed and PCS, respectively.

the process of point cloud restoration, and the watershed algorithm is better than the PCS method in segmentation

when the CHM is smoothed by a Gaussian filter. Under the optimal segmentation algorithm for different tree species,
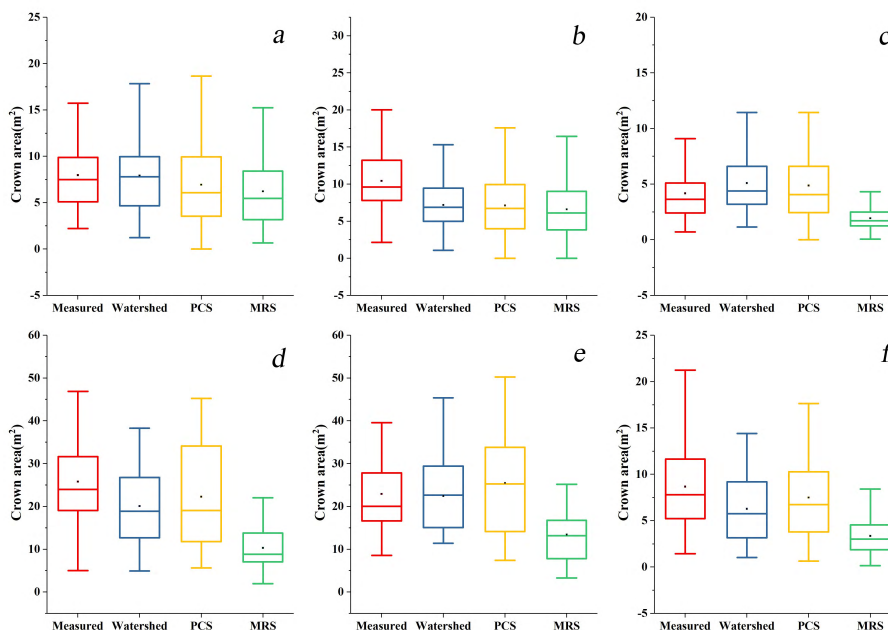
FIGURE 9. Results of individual tree crown areas in different sample plots. (a), (b) and (c) are the comparison between the crown areas of L1, L2, and L3 based on measured and different segmentation algorithms; (d), (e) and (f) are the comparison between the crown areas of P1, P2, and P3 based on measured values and different segmentation algorithms.
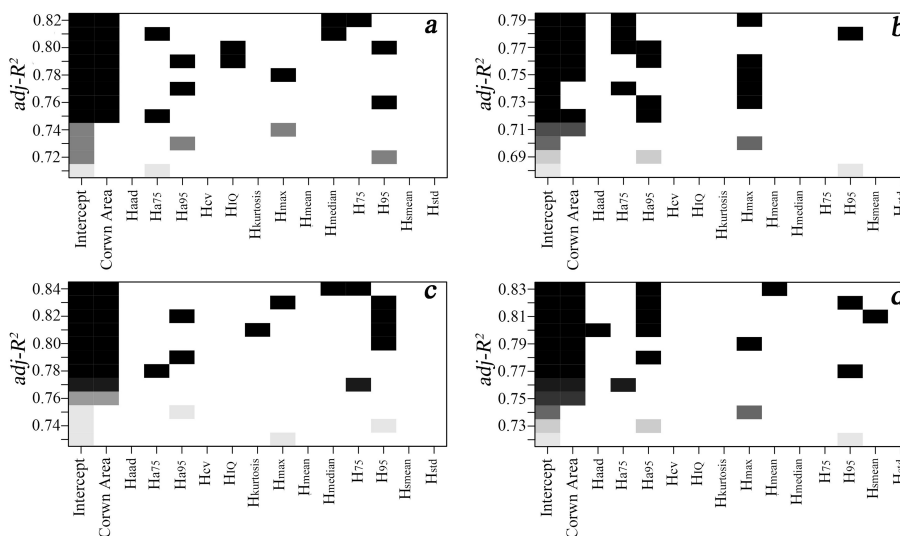
FIGURE 10. Results of stepwise regression for selecting the combination variables of the optimal models.

the overall segmentation accuracy of mature forests is better than that of young forests. Due to the large planted density of young forests and the fact that there are branching trees in the young larch sample plot, the branching tree crown is small and centralized, which increases the difficulty of automatic crown segmentation. Wallace *et al.* (2016) obtained LiDAR point clouds and high-resolution images of eucalyptus at an ultralow altitude (45 m) using a UAV and found that the two methods can provide terrain and canopy feature information in low canopy cover areas [50]. This finding is consistent with

the result showing that the segmentation accuracy of mature forests with relatively low canopy cover is higher than that of young forests. Compared with the research areas of Wallace and others, the study area in this study has a higher canopy cover, which may lead to the accuracy of MRS being lower than that of PCS. However, compared with larch, Chinese pine features some flat branches, thick twigs, and overlapping crowns of adjacent trees. The mean values of bands in the orthophoto image vary little, which results in some under-segmentation, and the segmentation accuracy of Chinese pine
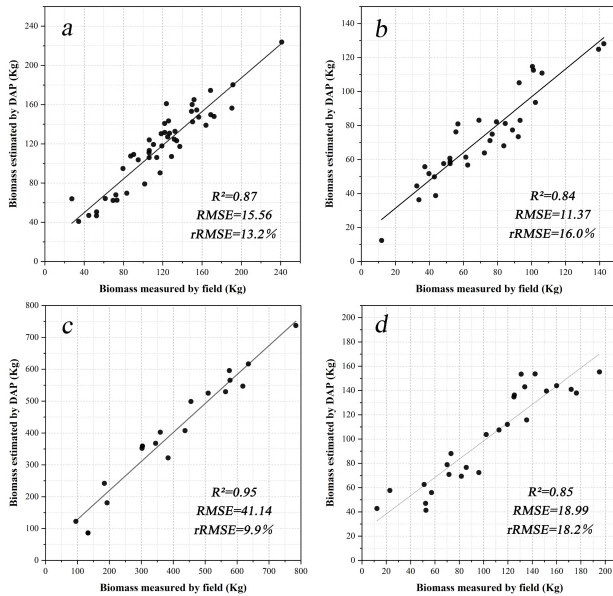
FIGURE 11. Accuracy verification results of the optimal models. (a), (b), (c) and (d) are the verification results of the biomass of mature larch, young larch, mature Chinese pine and young Chinese pine, respectively.

(average F-score = 0.83) is generally lower than that of larch (average F-score = 0.92). In the future, we plan to explore the impact of UAV flight height and tilt angle of the camera on obtaining forest vertical structure information and potential improvements in UAV oblique photography techniques for detecting trees in a forest. Additionally, we may explore a combination of oblique photography data with terrestrial laser scanning or close-range photography data to achieve the purpose of improving the accuracy of individual tree segmentation by combining information on the low levels of the forest with information on the canopy.

C. ACCURACY COMPARISON AND APPLICATION POTENTIAL OF INDIVIDUAL TREE PARAMETERS EXTRACTED BY UAV OBLIQUE PHOTOGRAPHY

The accuracy of tree height extraction was similar to that of segmentation for the trees of different ages. The accuracy of the individual tree height extraction of larch and Chinese pine is relatively good (average rRMSE = 6.12%), and the tree height extraction accuracy of the mature forests (average RMSE = 0.79 m, rRMSE $\leq$ 5.0%) is higher than that of the young forests (average RMSE = 1.25 m, rRMSE$\leq$12.2%). This is similar to the results of Edson *et al.* (2011), whose research showed that the accuracy is lower for young tree plots than old tree plots based on LiDAR point cloud data extraction [51]. The canopies of mature forests have clear borders and relatively low densities, while young forests have higher densities; thus, mismatches are more likely to occur when recovering 3D point clouds of young forests. The PCS algorithm is suitable for extracting individual tree heights of mature larch and mature and young Chinese pine, and the

watershed algorithm is suitable for extracting individual tree heights of young larch.

In terms of crown area extraction, the accuracy of the watershed and PCS methods is better than that of MRS. The canopy segmented by MRS excludes the influence of the ground background, and the compactness of the crown boundary is high, resulting in a crown area that is smaller than the measured value. On the other hand, the calculation of the measured crown area uses the average length in the north-south and east-west directions as the diameter to calculate the circular area, which results in the measured area being larger than the actual canopy area. In addition, there is an error in the artificial estimation in field measurements. All of the above might lead to such results. Panagiotidis *et al.* (2017) successfully estimated the height and crown diameter of individual trees in European coniferous forests based on high-resolution UAV images [52], their success might be because their study area was a mixed forest, whereas the study area in this paper is a pure forest, which leads to the lower precision of the individual tree height extraction (rRMSE = 11.42 $\sim$ 12.62). The selection of crown width as the evaluation indicator of canopy extraction might result in a crown area accuracy (rRMSE = 14.29 $\sim$ 18.56) that is better than that extracted in this paper.

In this study, the parameters of larch and Chinese pine in northern China were extracted using UAV oblique photography. The results show that the low-cost UAV oblique photography technique performs well in the extraction of individual tree parameters and can meet the daily demand of forestry production and can be applied to achieve large-scale biomass estimation. Because the canopy cover of the sample plots in this study is relatively large, oblique photogrammetry technology cannot detect all the information of the low levels of the forest, so when selecting the metrics of point clouds, the metrics with strong correlation with tree height (such as the percentile of the upper height, the coefficient of height variation, the median of point cloud height and other metrics) should be selected. The crown area can be extracted by segmentation and has a strong correlation with biomass; therefore, it was used as an independent variable together with point cloud metrics in the fitting of individual tree biomass prediction models. The independent variables with the highest correlation are combined into the optimal models (average R^2 = 0.88, average rRMSE = 14.3%). Lin *et al.* (2018) successfully estimated the biomass of Cunninghamia lanceolata (Lamb.) Hook. (R^2 = 0.96, RMSE = 54.90 kg) [25]. Jing *et al.* (2017) successfully estimated the aboveground biomass of aquatic plants (R^2 = 0.84, RMSE = 7.13%) [42] based on the regression model of height variables and vegetation index extracted from a point cloud and orthophoto images recovered with the SFM technique.

V. CONCLUSION

In this study, high-resolution oblique photographs of larch and Chinese pine in mature and young stands collected with a UAV were used to generate orthophoto images and 3D point

clouds for the flight area using the SFM technique. A DSM was generated using IDW interpolation. The watershed, PCS and MRS methods were used to segment individual trees and extract individual tree parameters for 188 mature larch trees, 139 young larch trees, 64 mature Chinese pine trees and 117 young Chinese pine trees. Biomass models were generated for individual trees of mature and young Chinese pine, and their accuracy was assessed. The results are as follows: PCS is suitable for individual larch segmentation (average F-score = 0.94), tree height extraction of mature larch and mature and young Chinese pine (average rRMSE = 3.9%, 4.3%, 9.8%), and crown area extraction of young Chinese pine (rRMSE = 33.5%). The watershed algorithm is suitable for individual Chinese pine segmentation (average F-score = 0.89), tree height extraction of young larch (rRMSE = 7.4%), and crown area extraction of larch and young Chinese pine (rRMSE = 33.5%). The stepwise regression method was used to fit the individual tree biomass models, and the coefficients of determination (R^2) of the models are all greater than 0.8, which shows that the combination of individual tree point cloud metrics and crown area can effectively fit the biomass model of larch and Chinese pine. This study shows that UAV oblique photography has good effects in terms of individual tree identification for larch and Chinese pine plantation forests in northern China and has good potential for the extraction of individual tree parameters.

REFERENCES

[1] S. Sakurai, "Plantation forestry in the tropics," in *Plantation Technology in Tropical Forest Science*. Tokyo, Japan: Springer, 2006, pp. 53–63, doi: 10.1007/4-431-28054-5_5.

[2] G. Pinjuv, E. G. Mason, and M. Watt, "Quantitative validation and comparison of a range of forest growth model types," *Forest Ecol. Manage.*, vol. 236, no. 1, pp. 37–46, Nov. 2006, doi: 10.1016/j.foreco.2006.06.025.

[3] M. Sprintsin, A. Karnieli, P. Berliner, E. Rotenberg, D. Yakir, and S. Cohen, "The effect of spatial resolution on the accuracy of leaf area index estimation for a forest planted in the desert transition zone," *Remote Sens. Environ.*, vol. 109, no. 4, pp. 416–428, Aug. 2007, doi: 10.1016/j.rse.2007.01.020.

[4] B. Apostol, M. Petrila, A. Lorenţ, A. Ciceu, V. Gancz, and O. Badea, "Species discrimination and individual tree detection for predicting main dendrometric characteristics in mixed temperate forests by use of airborne laser scanning and ultra-high-resolution imagery," *Sci. Total Environ.*, vol. 698, Jan. 2020, Art. no. 134074, doi: 10.1016/j.scitotenv.2019.134074.

[5] X. Wu, X. Shen, L. Cao, G. Wang, and F. Cao, "Assessment of individual tree detection and canopy cover estimation using unmanned aerial vehicle based light detection and ranging (UAV-LiDAR) data in planted forests," *Remote Sens.*, vol. 11, no. 8, p. 908, Apr. 2019, doi: 10.3390/rs11080908.

[6] T. Sankey, J. Donager, J. McVay, and J. B. Sankey, "UAV LiDAR and hyperspectral fusion for forest monitoring in the southwestern USA," *Remote Sens. Environ.*, vol. 195, pp. 30–43, Jun. 2017, doi: 10.1016/j.rse.2017.04.007.

[7] C. A. Silva, C. Klauberg, Â. M. K. Hentz, A. P. D. Corte, U. Ribeiro, and V. Liesenberg, "Comparing the performance of ground filtering algorithms for terrain modeling in a forest environment using airborne LiDAR data," *Floresta Ambiente*, vol. 25, no. 2, pp. 1–10, Feb. 2018, doi: 10.1590/2179-8087.015016.

[8] Q. Liu, S. Li, Z. Li, L. Fu, and K. Hu, "Review on the applications of UAV-based LiDAR and photogrammetry in forestry," *Linye Kexue/Scientia Silvae Sinicae*, vol. 53, no. 7, pp. 134–148, 2017, doi: 10.11707/j.1001-7488.20170714.

[9] R. H. Waring, N. C. Coops, and J. J. Landsberg, "Improving predictions of forest growth using the 3-PGS model with observations made by remote sensing," *Forest Ecol. Manage.*, vol. 259, no. 9, pp. 1722–1729, Apr. 2010, doi: 10.1016/j.foreco.2009.05.036.

[10] J. C. White, P. Tompalski, N. C. Coops, and M. A. Wulder, "Comparison of airborne laser scanning and digital stereo imagery for characterizing forest canopy gaps in coastal temperate rainforests," *Remote Sens. Environ.*, vol. 208, pp. 1–14, Apr. 2018, doi: 10.1016/j.rse.2018.02.002.

[11] S. Tao, Q. Guo, L. Li, B. Xue, M. Kelly, W. Li, G. Xu, and Y. Su, "Airborne LiDAR-derived volume metrics for aboveground biomass estimation: A comparative assessment for conifer stands," *Agricult. Forest Meteorol.*, vols. 198–199, pp. 24–32, Nov. 2014.

[12] Q. Chen, D. Baldocchi, P. Gong, and M. Kelly, "Isolating individual trees in a savanna woodland using small footprint LiDAR data," *Photogramm. Eng. Remote Sens.*, vol. 72, no. 8, pp. 923–932, Aug. 2006, doi: 10.14358/PERS.72.8.923.

[13] W. Chen, H. Xiang, and K. Moriya, "Individual tree position extraction and structural parameter retrieval based on airborne LiDAR data: Performance evaluation and comparison of four algorithms," *Remote Sens.*, vol. 12, no. 3, p. 571, Feb. 2020, doi: 10.3390/rs12030571.

[14] A. P. Nyaruhuma, M. Gerke, G. Vosselman, and E. G. Mtalo, "Verification of 2D building outlines using oblique airborne images," *ISPRS J. Photogramm. Remote Sens.*, vol. 71, pp. 62–75, Jul. 2012, doi: 10.1016/j.isprsjprs.2012.04.007.

[15] J. White, C. Stepper, P. Tompalski, N. Coops, and M. Wulder, "Comparing ALS and image-based point cloud metrics and modelled forest inventory attributes in a complex coastal forest environment," *Forests*, vol. 6, no. 12, pp. 3704–3732, Oct. 2015, doi: 10.3390/f6103704.

[16] J. C. White, N. C. Coops, M. A. Wulder, M. Vastaranta, T. Hilker, and P. Tompalski, "Remote sensing technologies for enhancing forest inventories: A review," *Can. J. Remote Sens.*, vol. 42, no. 5, pp. 619–641, Sep. 2016, doi: 10.1080/07038992.2016.1207484.

[17] J. Zhang, J. Hu, J. Lian, Z. Fan, X. Ouyang, and W. Ye, "Seeing the forest from drones: Testing the potential of lightweight drones as a tool for long-term forest monitoring," *Biol. Conservation*, vol. 198, pp. 60–69, Jun. 2016, doi: 10.1016/j.biocon.2016.03.027.

[18] J. P. Dash, M. S. Watt, G. D. Pearse, M. Heaphy, and H. S. Dungey, "Assessing very high resolution UAV imagery for monitoring forest health during a simulated disease outbreak," *ISPRS J. Photogramm. Remote Sens.*, vol. 131, pp. 1–14, Sep. 2017, doi: 10.1016/j.isprsjprs.2017.07.007.

[19] J. Lisein, M. Pierrot-Deseilligny, S. Bonnet, and P. Lejeune, "A photogrammetric workflow for the creation of a forest canopy height model from small unmanned aerial system imagery," *Forests*, vol. 4, no. 4, pp. 922–944, Nov. 2013, doi: 10.3390/f4040922.

[20] L. Cao, H. Liu, X. Fu, Z. Zhang, X. Shen, and H. Ruan, "Comparison of UAV LiDAR and digital aerial photogrammetry point clouds for estimating forest structural attributes in subtropical planted forests," *Forests*, vol. 10, no. 2, pp. 1–26, 2019, doi: 10.3390/f10020145.

[21] J. Jensen and A. Mathews, "Assessment of image-based point cloud products to generate a bare earth surface and estimate canopy heights in a woodland ecosystem," *Remote Sens.*, vol. 8, no. 1, p. 50, Jan. 2016, doi: 10.3390/rs8010050.

[22] T. R. H. Goodbody, N. C. Coops, P. Tompalski, P. Crawford, and K. J. K. Day, "Updating residual stem volume estimates using ALS- and UAV-acquired stereo-photogrammetric point clouds," *Int. J. Remote Sens.*, vol. 38, nos. 8–10, pp. 2938–2953, May 2017, doi: 10.1080/01431161.2016.1219425.

[23] F. Giannetti, G. Chirici, T. Gobakken, E. Næsset, D. Travaglini, and S. Puliti, "A new approach with DTM-independent metrics for forest growing stock prediction using UAV photogrammetric data," *Remote Sens. Environ.*, vol. 213, pp. 195–205, Aug. 2018, doi: 10.1016/j.rse.2018.05.016.

[24] J. Guerra-Hernández, E. González-Ferreiro, V. J. Monleón, S. P. Faias, M. Tomé, and R. A. Díaz-Varela, "Use of multi-temporal UAV-derived imagery for estimating individual tree growth in Pinus pinea stands," *Forests*, vol. 8, no. 8, pp. 1–19, 2017, doi: 10.3390/f8080300.

[25] J. Lin, M. Wang, M. Ma, and Y. Lin, "Aboveground tree biomass estimation of sparse subalpine coniferous forest with UAV oblique photography," *Remote Sens.*, vol. 10, no. 11, p. 1849, Nov. 2018, doi: 10.3390/rs10111849.

[26] P. Shin, T. Sankey, M. M. Moore, and A. E. Thode, "Evaluating unmanned aerial vehicle images for estimating forest canopy fuels in a ponderosa pine stand," *Remote Sens.*, vol. 10, no. 8, pp. 3–5, 2018, doi: 10.3390/rs10081266.

[27] D. R. Miller, C. P. Quine, and W. Hadley, "An investigation of the potential of digital photogrammetry to provide measurements of forest characteristics and abiotic damage," *Forest Ecol. Manage.*, vol. 135, nos. 1–3, pp. 279–288, 2000, doi: 10.1016/S0378-1127(00)00286-3.

[28] D. Turner, A. Lucieer, and C. Watson, "An automated technique for generating georectified mosaics from ultra-high resolution unmanned aerial vehicle (UAV) imagery, based on structure from motion (SfM) point clouds," *Remote Sens.*, vol. 4, no. 5, pp. 1392–1410, May 2012, doi: 10.3390/rs4051392.

[29] M. I. A. Lourakis and A. A. Argyros, "SBA: A software package for generic sparse bundle adjustment," *ACM Trans. Math. Softw.*, vol. 36, no. 1, pp. 1–30, Mar. 2009.

[30] M. Vastaranta, M. A. Wulder, J. C. White, A. Pekkarinen, S. Tuominen, C. Ginzler, V. Kankare, M. Holopainen, J. Hyyppä, and H. Hyyppä, "Airborne laser scanning and digital stereo imagery measures of forest structure: Comparative results and implications for forest mapping and inventory update," *Can. J. Remote Sens.*, vol. 39, no. 5, pp. 382–395, Nov. 2013, doi: 10.5589/m13-046.

[31] H. Huang, X. Li, and C. Chen, "Individual tree crown detection and delineation from very-high-resolution UAV images based on bias field and marker-controlled watershed segmentation algorithms," *IEEE J. Sel. Topics Appl. Earth Observ. Remote Sens.*, vol. 11, no. 7, pp. 2253–2262, Jul. 2018, doi: 10.1109/JSTARS.2018.2830410.

[32] L. Vincent and P. Soille, "Watersheds in digital spaces: An efficient algorithm based on immersion simulations," *IEEE Trans. Pattern Anal. Mach. Intell.*, vol. 13, no. 6, pp. 583–598, Jun. 1991.

[33] W. Li, Q. Guo, M. K. Jakubowski, and M. Kelly, "A new method for segmenting individual trees from the LiDAR point cloud," *Photogramm. Eng. Remote Sens.*, vol. 78, no. 1, pp. 75–84, Jan. 2012, doi: 10.14358/PERS.78.1.75.

[34] A. Tzotsos, C. Iosifidis, and D. Argialas, "A hybrid texture-based and region-based multi-scale image segmentation algorithm," in *Object-Based Image Analysis*. Berlin, Germany: Springer, 2008.

[35] A. R. Rivera, B. Ryu, and O. Chae, "Content-aware dark image enhancement through channel division," *IEEE Trans. Image Process.*, vol. 21, no. 9, pp. 3967–3980, Sep. 2012.

[36] C. J. Veenman and M. J. T. Reinders, "The nearest subclass classifier: A compromise between the nearest mean and nearest neighbor classifier," *IEEE Trans. Pattern Anal. Mach. Intell.*, vol. 27, no. 9, pp. 1417–1429, Sep. 2005, doi: 10.1109/TPAMI.2005.187.

[37] N. Wolf, "Object features for pixel-based classification of urban areas comparing different machine learning algorithms," *Photogramm. Fernerkundung, Geoinf.*, vol. 2013, no. 3, pp. 149–161, 2013, doi: 10.1127/1432-8364/2013/0166.

[38] J.-M. Yang, P.-T. Yu, and B.-C. Kuo, "A nonparametric feature extraction and its application to nearest neighbor classification for hyperspectral image data," *IEEE Trans. Geosci. Remote Sens.*, vol. 48, no. 3, pp. 1279–1293, Mar. 2010, doi: 10.1109/TGRS.2009.2031812.

[39] F. A. Gougeon, "A crown-following approach to the automatic delineation of individual tree crowns in high spatial resolution aerial images," *Can. J. Remote Sens.*, vol. 21, no. 3, pp. 274–284, Aug. 1995.

[40] C. Goutte and E. Gaussier, "A probabilistic interpretation of precision, recall and F-score, with implication for evaluation," in *Proc. Eur. Conf. Inf. Retr.*, in Lecture Notes in Computer Science, vol. 3408, 2005, pp. 345–359, doi: 10.1007/978-3-540-31865-1_25.

[41] M. Sokolova, N. Japkowicz, and S. Szpakowicz, "Beyond accuracy, F-score and ROC: A family of discriminant measures for performance evaluation," in *Proc. Australas. Joint Conf. Artif. Intell.*, in Lecture Notes in Computer Science, vol. 4304, 2006, pp. 1015–1021.

[42] R. Jing, Z. Gong, W. Zhao, R. Pu, and L. Deng, "Above-bottom biomass retrieval of aquatic plants with regression models and SfM data acquired by a UAV platform—A case study in wild duck lake wetland, Beijing, China," *ISPRS J. Photogramm. Remote Sens.*, vol. 134, pp. 122–134, Dec. 2017, doi: 10.1016/j.isprsjprs.2017.11.002.

[43] Y. Luo, X. Wang, and F. Lu, *Comprehensive Database of Biomass Regressions for China's Tree Spieces*, 1st ed. Beijing, China: China Forestry Publishing House, Dec. 2015.

[44] Y. Lin, J. Hyyppa, and A. Jaakkola, "Mini-UAV-borne LiDAR for fine-scale mapping," *IEEE Geosci. Remote Sens. Lett.*, vol. 8, no. 3, pp. 426–430, May 2011.

[45] P. J. Zarco-Tejada, R. Diaz-Varela, V. Angileri, and P. Loudjani, "Tree height quantification using very high resolution imagery acquired from an unmanned aerial vehicle (UAV) and automatic 3D photo-reconstruction methods," *Eur. J. Agronomy*, vol. 55, pp. 89–99, Apr. 2014, doi: 10.1016/j.eja.2014.01.004.

[46] K. Liu, X. Shen, L. Cao, G. Wang, and F. Cao, "Estimating forest structural attributes using UAV-LiDAR data in ginkgo plantations," *ISPRS J. Photogramm. Remote Sens.*, vol. 146, pp. 465–482, Dec. 2018, doi: 10.1016/j.isprsjprs.2018.11.001.

[47] N. C. Coops, R. H. Waring, and J. J. Landsberg, "Estimation of potential forest productivity across the oregon transect using satellite data and monthly weather records," *Int. J. Remote Sens.*, vol. 22, no. 18, pp. 3797–3812, Jan. 2001, doi: 10.1080/01431160010014710.

[48] J. Mustonen, P. Packalén, and A. Kangas, "Automatic segmentation of forest stands using a canopy height model and aerial photography," *Scandin. J. Forest Res.*, vol. 23, no. 6, pp. 534–545, Dec. 2008, doi: 10.1080/02827580802552446.

[49] Z. A. Latif, S. N. A. Aman, and R. Ghazali, "Delineation of tree crown and canopy height using airborne LiDAR and aerial photo," in *Proc. IEEE 7th Int. Colloq. Signal Process. Appl.*, no. 2, Mar. 2011, pp. 354–358, doi: 10.1109/CSPA.2011.5759902.

[50] L. Wallace, A. Lucieer, Z. Malenovský, D. Turner, and P. Vopěnka, "Assessment of forest structure using two UAV techniques: A comparison of airborne laser scanning and structure from motion (SfM) point clouds," *Forests*, vol. 7, no. 3, pp. 1–16, 2016, doi: 10.3390/f7030062.

[51] C. Edson and M. G. Wing, "Airborne light detection and ranging (LiDAR) for individual tree stem location, height, and biomass measurements," *Remote Sens.*, vol. 3, no. 11, pp. 2494–2528, 2011.

[52] D. Panagiotidis, A. Abdollahnejad, P. Surový, and V. Chiteculo, "Determining tree height and crown diameter from high-resolution UAV imagery," *Int. J. Remote Sens.*, vol. 38, nos. 8–10, pp. 2392–2410, May 2017, doi: 10.1080/01431161.2016.1264028.

XUEMEI ZHOU received the B.S. degree in geographic information science from Anhui Normal University, China, in 2017. She has been studying cartography and geographic information system with Beijing Forestry University, Beijing, China, since September 2017. Her research interests include UAV oblique photogrammetry and forestry remote sensing. She designed the overall structure of the article and wrote the original draft.

XIAOLI ZHANG received the B.S. degree in computer science from Hebei University, Baoding, China, in 1989, and the Ph.D. degree in forest management science from Beijing Forestry University, Beijing, China, in 1998.

From 2006 to 2007, she was a Visiting Scholar in remote sensing and intelligent analysis at Lincoln University, New Zealand. From 1989 to 1992, she was an Assistant with the Mathematics Department, Zhangjiakou Normal College, China. From 1998 to 1999, she was a Postdoctoral Research Fellow with the Institute of Remote Sensing Application, CAS, Beijing. From 1999 to 2006, she was an Associate Professor with the College of Forestry, Beijing Forestry University, Beijing, where she has been a Professor, since 2007. Her recently published articles are as follows, Assessing the defoliation of pine forests in a long time-series and spatiotemporal prediction of the defoliation using Landsat data (2018), (with Zhu, C., Zhang, X., Zhang, N., Hassan, M., and Zhao, L.), and Assessment of defoliation during Dendrolimus tabulaeformis Tsai et Liu disaster outbreak using UAV-based hyperspectral image (2018), (with Zhang, N., Zhang, X., Yang, G., Zhu, C., Huo, L., and Feng, H.) in *Remote Sensing of Environment*. Her research interests include forest resources and ecological environment remote sensing monitoring and spatial prediction, forest disease and pest remote sensing monitoring and risk assessment, and vegetation quantitative remote sensing.

Prof. Zhang is a Councilor of the Associate on Environment Remote Sensing of China (AERSC), a Supervisor of Beijing Society for Information Technology in Agriculture, and a member of Forest Management Branch of Chinese Society of Forestry. Her awards and honors include the National Scientific and Technological Progress Award, the MOE Scientific and Technological Progress Award, the Beijing Science and Technology Award, the Forest Science and Technology Award for Chinese Youth, and the MOE New Century Excellent Talents (NCET).

• • •